Backbending in the pear-shaped $^{223}_{90}$Th nucleus: Evidence of a high-spin octupole to quadrupole shape transition in the actinides

G. Maquart,[1] L. Augey,[1,*] L. Chaix,[1,†] I. Companis,[1] C. Ducoin,[1] J. Dudouet,[1] D. Guinet,[1] G. Lehaut,[1,*] C. Mancuso,[1] N. Redon,[1] O. Stézowski,[1] A. Vancraeyenest,[1] A. Astier,[2] F. Azaiez,[3] S. Courtin,[4] D. Curien,[4] I. Deloncle,[2] O. Dorvaux,[4] G. Duchêne,[4] B. Gall,[4] T. Grahn,[5] P. Greenlees,[5] A. Herzan,[5] K. Hauschild,[2] U. Jakobsson,[5] P. Jones,[3,5] R. Julin,[5] S. Juutinen,[5] S. Ketelhut,[5] M. Leino,[5] A. Lopez-Martens,[5] P. Nieminen,[5] P. Petkov,[2,6] P. Peura,[5] M.-G. Porquet,[2] P. Rahkila,[5] S. Rinta-Antila,[5] M. Rousseau,[4] P. Ruotsalainen,[5] M. Sandzelius,[5] J. Sarén,[5] C. Scholey,[5] J. Sorri,[5] S. Stolze,[5] and J. Uusitalo[5]

[1]*IPNL, CNRS/IN2P3, Université de Lyon/UCBL, F69622 Villeurbanne Cedex, France*

[2]*CSNSM, CNRS/IN2P3, Université Paris Sud, 91405 Orsay, France*

[3]*iThemba LABS, P.O. Box 722, Somerset West, 7129, South Africa*

[4]*CNRS/IN2P3, IPHC UMR 7178, F-67037 Strasbourg, France*

[5]*University of Jyväskylä, Department of Physics, P.O. Box 35, FI-40014 University of Jyväskylä, Finland*

[6]*INRNE, Bulgarian Academy of Science, 1784 Sofia, Bulgaria*

(Received 1 December 2016; published 6 March 2017)

Relatively neutron-rich thorium isotopes lie at the heart of a nuclear region of nuclei exhibiting octupole correlation effects. The detailed level structure of ^{223}Th has been investigated in measurements of γ radiation following the fusion-evaporation channel of the ^{208}Pb(^{18}O ,$3n$)^{223}Th reaction at 85 MeV beam energy. The level structure has been extended up to spin 49/2, and 33 new γ rays have been added using triple-γ coincidence data. The spins and parities of the newly observed states have been confirmed by angular distribution ratios. In addition to the two known yrast bands based on a $K = 5/2$ configuration, a non-yrast band has been established up to spin 35/2. We interpret this new structure as based on the same configuration as the yrast band in ^{221}Th having dominant $K = 1/2$ contribution. At the highest spin a backbending occurs around a rotational frequency of $\hbar\omega = 0.23$ MeV, very close to the one predicted in ^{222}Th, where a sharp transition to a reflection-symmetric shape is expected.

DOI: 10.1103/PhysRevC.95.034304

I. INTRODUCTION

In many aspects, the actinide region (from Rn to Th) presents a rich variety of phenomena connected with the octupole degree of freedom, which can form, for instance, pear-shaped nuclei [1–3]. It is well known from molecular spectroscopy that reflection-asymmetry induces rotational bands composed of alternating parity states connected by strong, collective, $E1$ transitions. The same situation occurs in the spectrum of octupole nuclei; however, in nuclear spectroscopy, the separation between rotational and vibrational collective modes is less clear than in molecules. Band heads could vary from vibration-like structure to static octupole shape depending on the potential energy surfaces at spin zero.

Focusing on thorium isotopes, recent calculations [4,5] suggest a rapid shape evolution from a spherical ground state in ^{220}Th to a pronounced quadrupole-octupole deformation in ^{228}Th. This evolution is identified as a double shape phase transition occurring as the neutron number N (control parameter) increases: a transition from spherical to quadrupole shape, and a transition from nonoctupole to octupole shape. Observables associated with order parameters for both changes present a sudden evolution around $N = 134$, putting ^{224}Th at the heart of this double phase transition.

In the framework of covariant density functional theory, Agbemava *et al.* [6] support such a rapid evolution by calculating the equilibrium deformations β_2, β_3 and the gain of binding energy due to octupole deformation. Their study also points out the effect of pairing at low spin. Although the topology of the potential energy surfaces is not drastically modified by changes in the pairing strength, it appears that a weaker pairing is more favorable to octupole deformation. For instance, in the case of the octupole nucleus ^{224}Th, the potential energy surface presents two minima, corresponding respectively to pure quadrupole and quadrupole-octupole deformation. A stronger pairing weakens the octupole rigidity in two ways: the energy difference between octupole and quadrupole minima is reduced, and so is the height of the potential barrier between them. Therefore, they concluded that the strongest impact due to the octupole degree of freedom is expected in the systems with weakest pairing. Because of the level blocking that weakens the pairing effects in odd-mass systems, we may expect a stronger presence of octupolarity in odd-mass nuclei such as ^{223}Th. However, the additional coupling of the quasiparticle to deformation and rotation has to be taken into account [7]. Characteristics of rotational bands, at medium and high spin, would also reveal how the shape competition evolves with collective rotations.

The decay scheme of ^{223}Th is one of the most relevant examples of a nuclear high-spin-parity doublet [1,8]. In this

*Present address: LPC, ENSICAEN, CNRS/IN2P3, Université de Caen, 14050 Caen Cedex, France.

†Present address: Stanford Institute for Materials and Energy Sciences, SLAC National Accelerator Laboratory and Stanford University, 2575 Sand Hill Road, Menlo Park, California 94025, USA.

work, we have extended the level structure of ^{223}Th up to spin 49/2, and 33 new transitions have been added in the level scheme. A new, non-yrast, structure at low spin has been established. The new band does not show the typical interlinked bands with opposite simplex and is interpreted as being based on a dominant $K = 1/2$ contribution. The known rotational bands with $K = 5/2$ configuration have been extended up to very high spin, allowing us to observe for the first time a backbending that is interpreted as a band crossing.

II. EXPERIMENTAL DETAILS

A. Experimental setup

The ^{223}Th nuclei were produced by the fusion-evaporation reaction ^{208}Pb(^{18}O,$3n$)^{223}Th. This reaction was performed using an 85 MeV ^{18}O beam delivered by the Vivitron tandem of Institut de Recherches Subatomiques (IReS), Strasbourg, impinged on a 100 mg cm^{-2} ^{208}Pb self-supporting target where the beam was stopped. The incident energy thus covered a wide range, giving rise to different reaction types. The experiment was initially dedicated to the study of high-spin states in fission fragments. However, the analysis of these data has revealed interesting features in nuclei produced in different reaction channels with high statistics. For instance, Doppler shifted γ rays emitted by the ^{212}Po nucleus produced by α transfer have been assigned to enhanced $E1$ transitions from non-natural parity levels, leading to the discovery of a new kind of cluster structures [9–11]. ^{223}Th is one of the most produced nuclei in this experiment, which reflects the dominant contribution of the (^{18}O,$3n$) reaction channel at the energy where fusion is favored. One can notice that a similar reaction was used in Ref. [8] to produce ^{223}Th nuclei, while mainly ^{221}Th nuclei were obtained by using instead either an ^{16}O beam [12] or a ^{207}Pb target [13].

The γ rays produced by the deexcitation of ^{223}Th were detected by the EUROBALL IV array [14], composed of 71 Compton-suppressed germanium detectors disposed around the target as follows:

(1) At backward angles: 15 cluster detectors, each composed in 7 Ge crystals [15].
(2) Around 90 degrees: 26 clover detectors, each composed of 4 Ge crystals [16].
(3) At forward angles: 30 single-crystal tapered detectors.

The 239 crystals formed 13 rings at angles ranging from 15.5° to 163.5°.

Since the experiment was set up to study high-spin states involved in γ cascades of high-multiplicities, events were recorded only for γ multiplicities $\geqslant 3$ (namely, if at least three unsuppressed γ rays were observed in prompt coincidence). Under this condition, the recorded data set contains $\sim 4 \times 10^9$ events with fold $\geqslant 3$ and $\sim 1.8 \times 10^9$ with fold $\geqslant 4$ (from which we can estimate the production cross section to be $\sigma_{^{223}\mathrm{Th}} \simeq$ 1–10 mb).

B. Data analysis

We have investigated the structure of ^{223}Th by γ spectroscopy, using the multi-γ-ray coincidence technique to select the emitting nucleus and locate the observed transitions in its level scheme. The events recorded during the experiment were used to build multidimensional γ matrices counting the coincidences occurring between three or four γ rays (these matrices are denoted respectively cubes and hypercubes). Matrix projections under different sets of conditions produced multigated γ-ray spectra, obtained in the framework of the RADWARE package [17]. For instance, four-dimensional γ matrices (hypercubes) could be used to produce triple-gated spectra such as those shown in Fig. 1.

When allowed by the statistics, anisotropy measurements were used to determine the multipolarity of the transitions. For this purpose, the γ detectors were grouped into two parts centered at two mean angles: tapered plus cluster detectors ($T + C$) centered on 39.3°, and clover detectors (Q) centered on 76.6°. A symmetry around 90° with respect to the beam axis is assumed. The emitting nucleus is stopped in the target within a timescale of few picoseconds [11], shorter than the typical half-lives of the levels populated in ^{223}Th (no Doppler effect was observed for the γ rays emitted by this nucleus). The angular distribution ratio R_{ADO} (angular distribution from oriented nuclei) is given for each γ ray by

$$R_{\mathrm{ADO}} = \frac{I_\gamma(39.3\,\mathrm{deg})}{I_\gamma(76.6\,\mathrm{deg})} = \frac{I_\gamma(T+C)}{I_\gamma(Q)} \qquad (1)$$

The theoretical ADO ratios of 0.85 and 1.30 are expected for pure stretched dipole and quadrupole transitions, respectively, in the ^{212}Po nucleus [11]. Transitions of well-known multipolarity (in the ^{212}Po as well as in the ^{223}Th nuclei) were used to check that the measured R_{ADO} allows us to discriminate between stretched $\Delta I = 1$ transitions ($R_{\mathrm{ADO}} < 1$) and stretched $\Delta I = 2$ transitions ($R_{\mathrm{ADO}} > 1$). This study confirms the J^π assignment of all new states relatively to the previous ones.

III. RESULTS AND DISCUSSION

A. Level scheme of ^{223}Th

The level scheme of ^{223}Th is known to exhibit typical features of an octupole nucleus, namely two nearly degenerate bands of alternating parity [8,18]. These two bands are distinguished by the simplex quantum number s, related to the spin I and the parity p by

$$ps = e^{i\pi I}, \qquad (2)$$

which means that, for odd-mass nuclei implying semi-integer spin values, the levels can be classified in four sequences of given simplex and parity:

$$\text{1a: } (s,p) = (-i,-), \quad I^\pi = \left(\tfrac{1}{2}+2n\right)^- = \tfrac{1}{2}^-, \tfrac{5}{2}^-, \ldots,$$
$$\text{1b: } (s,p) = (-i,+), \quad I^\pi = \left(\tfrac{3}{2}+2n\right)^+ = \tfrac{3}{2}^+, \tfrac{7}{2}^+, \ldots,$$
$$\text{2a: } (s,p) = (+i,-), \quad I^\pi = \left(\tfrac{3}{2}+2n\right)^- = \tfrac{3}{2}^-, \tfrac{7}{2}^-, \ldots,$$
$$\text{2b: } (s,p) = (+i,+), \quad I^\pi = \left(\tfrac{1}{2}+2n\right)^+ = \tfrac{1}{2}^+, \tfrac{5}{2}^+, \ldots.$$

In the case of ^{223}Th ($N = 133$), the ground state has been assigned a spin-parity of $5/2^+$ [8]. This value has not been measured directly, but it has been adopted by analogy

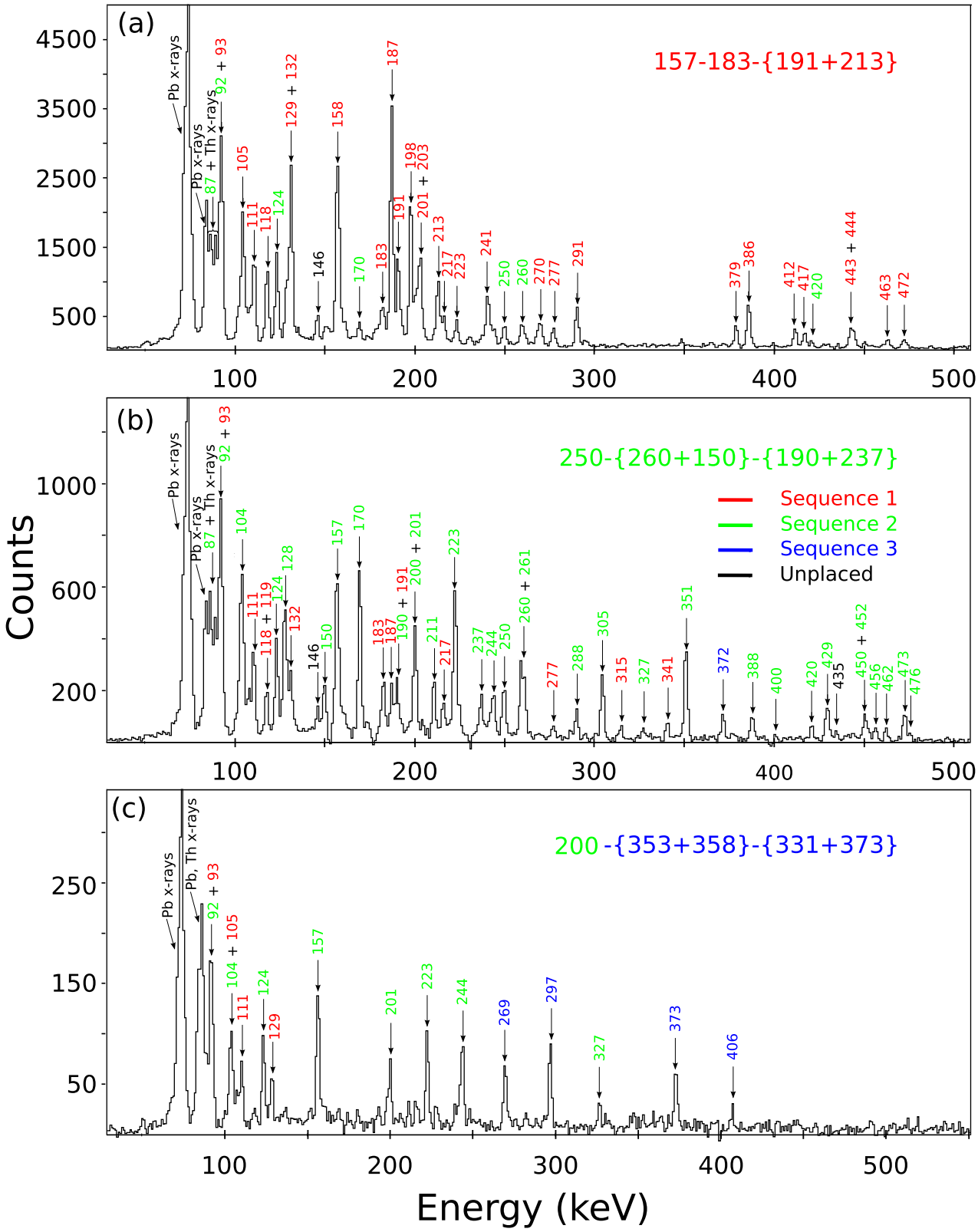

FIG. 1. Representative triple-gated spectra showing transitions between high-spin levels of ^{223}Th. Coincidence conditions are indicated. For instance, spectrum (a) shows the γ rays appearing in events for which the following set of transitions is also detected: 157 keV and 183 keV and (191 or 213) keV. The transitions of sequences 1a and 1b are indicated in red; sequences 2a and 2b in green; sequences 3a and 3b in blue. (a) Spectrum showing mostly transitions in sequences 1a and 1b. (b) Spectrum showing mostly transitions in sequences 2a and 2b. (c) Spectrum showing mostly transitions in sequences 3a and 3b. The presence of transitions from different bands in each spectrum is linked to the interband communication (see text).

with the radium isotone ^{221}Ra for which the spin and parity of the ground state ($5/2^+$) have been established by laser spectroscopic measurements [19]. This analogy is possible since both nuclei are expected to have similar deformation, and with an even proton number the spin-parity of the ground state is determined by the individual level occupied by the last neutron. Furthermore, the corresponding value is in agreement with theoretical calculations (see, e.g., Fig. 6 in Ref. [20], for an octupole deformation $\beta_3 \simeq 0.1$).

Most of the previous knowledge on the ^{223}Th level scheme was established by Dahlinger *et al.* [8]. We can also notice more recent measurements of low-spin states populated by α decay of ^{227}U [21,22]. Since the work presented in Ref. [8], the two principal bands of ^{223}Th were known up to the levels $31/2^+$ ($s = -i$) and $33/2^+$ ($s = +i$), although the transitions issuing from these last two levels could not be confirmed by γ-γ coincidences in the original experiment. In this previous work, the combination of electron and γ spectroscopy allowed the conversion coefficients associated with the transitions to be determined, and allowed the detection of strongly converted $M1$ transitions between the two bands of opposite simplex, which was not possible in the present analysis that is purely based on γ detection. Thus we have to keep in mind that the two bands communicate, although the corresponding transitions do not appear in the γ-ray spectra.

Seven weak transitions observed in Ref. [8] were attributed to ^{223}Th but could not be placed in the level scheme. The present analysis allowed us to identify two of them ($E_\gamma =$ 213.1 and 240.5 keV) as transitions between high-spin levels of the sequences 1a and 1b. A third one, at $E_\gamma = 146$ keV, seems to involve an unknown level offering an alternative path between the $17/2^-$ and $13/2^-$ levels of the sequence 1a. Indeed, it appears most strongly in coincidence with the transitions of this band, but is suppressed by a gate on known transitions between $17/2^-$ and $13/2^-$. Furthermore, it is emitted together with a γ ray at 77 keV different from the known transition between $13/2^+$ and $11/2^-$; since $E(17/2^-) - E(13/2^-) = 146 + 77$ keV, this supports the existence of such a new level (which would be situated at 401 or 470 keV depending on the ordering of the 146 and 77 keV transitions).

In the present work, 33 new γ rays from ^{223}Th have been observed, and 35 have been newly placed in the level scheme. The completion of the level scheme was performed on the basis of multi-γ coincidence analysis, together with intensity arguments. When allowed by the statistics, anisotropy measurements (R_{ADO}) were used to confirm the multipolarity of the transitions. The two principal bands of simplex $+i$ and $-i$ have been extended up to spin $43/2$ and $49/2$ respectively (14 new levels). The placement of the $31/2^+$ and $33/2^+$ levels proposed in Ref. [8] has been confirmed. In addition, a non-yrast structure previously unobserved has been constructed: it is composed of seven levels organized in two communicating bands, one of these bands being linked to the sequence 2b of the main structure. The list of observed γ transitions is given in Table I, ordered by energy.

The level scheme of ^{223}Th derived from this work is shown in Fig. 2. The arrows between the levels represent the γ intensity only (the contribution of internal conversion is not represented). The newly observed transitions that have been

TABLE I. Observed γ rays ordered by energy belonging to the ^{223}Th. Uncertainties in transition energies are typically between 0.1 and 0.5 keV. Intensities measured in this experiment are given with the requirement that a minimum of three unsuppressed Ge detectors fired in prompt coincidence. All γ intensities are normalized to the 123.5 keV transition. For total intensity, see [8] for cases in which a conversion coefficient has been calculated. Spin and parity are determined under the assumption that the spin-parity of the ground state is $\frac{5}{2}^+$. (○) The angular distribution ratio is calculated in the presence of an unresolved doublet. (∗) Tentative γ ray. (•) Unplaced transition.

E_γ (keV)	I_γ	R_{ADO}	ΔI	I_i^π	I_f^π	Localization
31.9	19(9)		1	$\frac{11}{2}^+$	$\frac{9}{2}^-$	1b–1a
51.3	7(2)		1	$\frac{7}{2}^+$	$\frac{5}{2}^+$	1b–2b
67.5	12(3)		1	$\frac{9}{2}^+$	$\frac{7}{2}^+$	2b–1b
76.8	63(12)		1	$\frac{13}{2}^+$	$\frac{11}{2}^-$	2b–2a
87.4	44(5)		1	$\frac{19}{2}^-$	$\frac{17}{2}^+$	2a–2b
92.3	83(12)		1	$\frac{15}{2}^-$	$\frac{13}{2}^+$	2a–2b
93.4	11(3)		1	$\frac{11}{2}^+$	$\frac{9}{2}^+$	1b–2b
103.8	36(14)	0.91(7)	1	$\frac{23}{2}^-$	$\frac{21}{2}^+$	2a–2b
104.8	45(14)	0.84(6)	1	$\frac{15}{2}^+$	$\frac{13}{2}^-$	1b–1a
108.6	10(5)		1	$\frac{13}{2}^+$	$\frac{11}{2}^+$	2b–1b
111.4	76(4)	0.63(7)	1	$\frac{13}{2}^-$	$\frac{11}{2}^+$	1a–1b
118.4	35(8)	0.73(7)	1	$\frac{17}{2}^-$	$\frac{15}{2}^+$	1a–1b
118.7	6(3)		2	$\frac{9}{2}^+$	$\frac{5}{2}^+$	2b–2b
123.5	77	0.88(8)	1	$\frac{11}{2}^-$	$\frac{9}{2}^+$	2a–2b
127.8	14(3)	0.87(7)	1	$\frac{27}{2}^-$	$\frac{25}{2}^+$	2a–2b
129.3	50(4)	0.67(7)	1	$\frac{9}{2}^-$	$\frac{7}{2}^+$	1a–1b
131.9	37(8)	0.72(7)	1	$\frac{21}{2}^-$	$\frac{19}{2}^+$	1a–1b
145.8(•)						linked to 1a
150.0	18(4)	0.84(8)	1	$\frac{31}{2}^-$	$\frac{29}{2}^+$	2a–2b
156.9	51(5)	0.81(7)	1	$\frac{17}{2}^+$	$\frac{15}{2}^-$	2b–2a
157.2	34(5)	0.73(7)	1	$\frac{25}{2}^-$	$\frac{23}{2}^+$	1a–1b
158.3	64(5)	0.69(8)	1	$\frac{19}{2}^+$	$\frac{17}{2}^-$	1b–1a
161.0	15(5)		2	$\frac{11}{2}^+$	$\frac{7}{2}^+$	1b–1b
169.0	8(4)	1.12(12)	2	$\frac{15}{2}^-$	$\frac{11}{2}^-$	2a–2a
169.6	10.6(24)	0.75(9)	1	$\frac{35}{2}^-$	$\frac{33}{2}^+$	2a–2b
183.1	38(9)	0.74(7)	1	$\frac{23}{2}^+$	$\frac{21}{2}^-$	1b–1a
187.3	49(3)	0.71(7)	1	$\frac{29}{2}^-$	$\frac{27}{2}^+$	1a–1b
190.0	5.3(15)	0.74(10)	1	$\frac{39}{2}^-$	$\frac{37}{2}^+$	2a–2b
191.1	38(3)	0.67(7)	1	$\frac{27}{2}^+$	$\frac{25}{2}^-$	1b–1a
197.8	25.3(37)	0.69(7)	1	$\frac{31}{2}^+$	$\frac{29}{2}^-$	1b–1a
200.3	44(3)	0.89(7)	1	$\frac{21}{2}^+$	$\frac{19}{2}^-$	2b–2a
200.9	18(2)		2	$\frac{13}{2}^+$	$\frac{9}{2}^+$	2b–2b
201.2	15.7(42)	0.63(10)	1	$\frac{39}{2}^+$	$\frac{37}{2}^-$	1b–1a
202.7	13.6(27)	0.73(10)	1	$\frac{35}{2}^+$	$\frac{33}{2}^-$	1b–1a
210.7	1.9(9)	0.65(1)	1	$\frac{43}{2}^-$	$\frac{41}{2}^+$	2a–2b
213.1	35.1(63)	0.76(7)	1	$\frac{33}{2}^-$	$\frac{31}{2}^+$	1a–1b
216.6	20(4)	1.03(7)	2	$\frac{15}{2}^+$	$\frac{11}{2}^+$	1b–1b

TABLE I. (*Continued.*)

E_γ (keV)	I_γ	R_{ADO}	ΔI	I_i^π	I_f^π	Localization
222.6	34(3)	0.77(7)	1	$\frac{25}{2}^+$	$\frac{23}{2}^-$	2b–2a
223.2			2	$\frac{17}{2}^-$	$\frac{13}{2}^-$	1a–1a
237.0	30(3)	0.87(8)	1	$\frac{29}{2}^+$	$\frac{27}{2}^-$	2b–2a
240.5	16.5(35)	0.82(8)	1	$\frac{37}{2}^-$	$\frac{35}{2}^+$	1a–1b
243.9	14(6)	1.26(9)	2	$\frac{19}{2}^-$	$\frac{15}{2}^-$	2a–2a
249.5	6(4)		2	$\frac{17}{2}^+$	$\frac{13}{2}^+$	2b–2b
250.0$^{(\circ)}$	25(5)	0.80(7)	1	$\frac{33}{2}^+$	$\frac{31}{2}^-$	2b–2a
250.0$^{(\circ)}$	3.4(14)	0.80(7)	1	$\frac{45}{2}^+$	$\frac{43}{2}^-$	2b–2a
259.5$^{(\circ)}$	10.4(29)	0.70(9)	1	$\frac{37}{2}^+$	$\frac{35}{2}^-$	2b–2a
260.5$^{(\circ)}$	6.4(17)	0.70(9)	1	$\frac{41}{2}^+$	$\frac{39}{2}^-$	2b–2a
268.7	16.1(43)	0.80(9)	1	$\frac{33}{2}^{(-)}$	$\frac{31}{2}^{(+)}$	3b–3a
269.8	7.8(22)	0.64(9)	1	$\frac{41}{2}^-$	$\frac{39}{2}^+$	1a–1b
276.9	10.7(25)	1.31(8)	2	$\frac{19}{2}^+$	$\frac{15}{2}^+$	1b–1b
288.4	3.9(9)	1.43(11)	2	$\frac{21}{2}^+$	$\frac{17}{2}^+$	2b–2b
290.5	15(2)	1.30(7)	2	$\frac{21}{2}^-$	$\frac{17}{2}^-$	1a–1a
296.8	9.2(26)	0.73(12)	1	$\frac{29}{2}^{(-)}$	$\frac{27}{2}^{(+)}$	3b–3a
300.8	10.5(34)	0.78(10)	1	$\frac{25}{2}^{(-)}$	$\frac{23}{2}^{(+)}$	3b–3a
305.2	19(2)	1.38(9)	2	$\frac{23}{2}^-$	$\frac{19}{2}^-$	2a–2a
315.2	4.8(9)	1.19(9)	2	$\frac{23}{2}^+$	$\frac{19}{2}^+$	1b–1b
326.6	4.4(18)	1.15(12)	2	$\frac{25}{2}^+$	$\frac{21}{2}^+$	2b–2b
331.4	6.5(24)	1.44(11)	2	$\frac{27}{2}^{(+)}$	$\frac{23}{2}^{(+)}$	3a–3a
340.7	8.1(27)	1.31(8)	2	$\frac{25}{2}^-$	$\frac{21}{2}^-$	1a–1a
348.6	10.8(36)	1.05(10)	2	$\frac{27}{2}^+$	$\frac{23}{2}^+$	1b–1b
351.0	19.9(54)	1.23(8)	2	$\frac{27}{2}^-$	$\frac{23}{2}^-$	2a–2a
353.3	11.6(19)	0.82(9)	1	$\frac{23}{2}^{(+)}$	$\frac{21}{2}^+$	3a–2b
357.9	8.0(17)	0.79(9)	1	$\frac{27}{2}^{(+)}$	$\frac{25}{2}^+$	3a–2b
365.5	9.2(22)	0.75(11)	1	$\frac{31}{2}^{(+)}$	$\frac{29}{2}^+$	3a–2b
366.2	9.1(27)	1.60(15)	2	$\frac{29}{2}^+$	$\frac{25}{2}^+$	2b–2b
371.7	3.4(10)	0.72(10)	1	$\frac{35}{2}^{(+)}$	$\frac{33}{2}^+$	3a–2b
373.1	9.3(23)	1.15(9)	2	$\frac{31}{2}^{(+)}$	$\frac{27}{2}^{(+)}$	3a–3a
378.6	9.2(28)	1.29(10)	2	$\frac{29}{2}^-$	$\frac{25}{2}^-$	1a–1a
386.0	4.6(19)	1.24(11)	2	$\frac{31}{2}^+$	$\frac{27}{2}^+$	1b–1b
387.7	11(3)	1.48(9)	2	$\frac{31}{2}^-$	$\frac{27}{2}^-$	2a–2a
400.3	12(3)	1.21(11)	2	$\frac{33}{2}^+$	$\frac{29}{2}^+$	2b–2b
(406.1)$^{(*)}$	5.0(35)	1.29(10)	2	$\frac{35}{2}^{(+)}$	$\frac{31}{2}^{(+)}$	3a–3a
411.5	7.1(13)	1.24(8)	2	$\frac{33}{2}^-$	$\frac{29}{2}^-$	1a–1a
416.9	10.6(25)	1.28(11)	2	$\frac{35}{2}^+$	$\frac{31}{2}^+$	1b–1b
420.1	8.0(19)	1.44(9)	2	$\frac{35}{2}^-$	$\frac{31}{2}^-$	2a–2a
428.8	8.8(22)	1.34(10)	2	$\frac{37}{2}^+$	$\frac{33}{2}^+$	2b–2b
434.7$^{(\bullet)}$	<0.8					
442.7$^{(\circ)}$	8.5(22)	1.34(9)	2	$\frac{39}{2}^+$	$\frac{35}{2}^+$	1b–1b
444.4$^{(\circ)}$	9.4(25)	1.34(9)	2	$\frac{37}{2}^-$	$\frac{33}{2}^-$	1a–1a
450$^{(\circ)}$	3.5(14)	1.34(10)	2	$\frac{39}{2}^-$	$\frac{35}{2}^-$	2a–2a
452$^{(\circ)}$	3.3(13)	1.34(10)	2	$\frac{41}{2}^+$	$\frac{37}{2}^+$	2b–2b

TABLE I. (*Continued.*)

E_γ (keV)	I_γ	R_{ADO}	ΔI	I_i^π	I_f^π	Localization
455.6	0.8(4)	1.29(15)	2	$\frac{49}{2}^+$	$\frac{45}{2}^+$	2b–2b
461.9	1.5(9)	1.18(13)	2	$\frac{45}{2}^+$	$\frac{41}{2}^+$	2b–2b
463.1	5.4(17)	1.13(11)	2	$\frac{43}{2}^+$	$\frac{39}{2}^+$	1b–1b
471.7	7.2(34)	1.17(12)	2	$\frac{41}{2}^-$	$\frac{37}{2}^-$	1a–1a
472.5	5.4(21)	1.62(11)	2	$\frac{43}{2}^-$	$\frac{39}{2}^-$	2a–2a
475.8	1.4(7)	1.52(18)	2	$\frac{47}{2}^-$	$\frac{43}{2}^-$	2a–2a
(487.9)$^{(*)}$	2.2(10)	1.38(13)	2	$\frac{45}{2}^-$	$\frac{41}{2}^-$	1a–1a

used to complete this scheme appear in the three γ spectra presented in Fig. 1. For each of these spectra, the gates have been chosen in order to highlight the transitions between high-spin levels of a given structure: respectively, the main band of simplex $-i$ (composed of the sequences 1a and 1b), the main band of simplex $+i$ (composed of the sequences 2a and 2b), and the non-yrast structure (composed of the sequences 3a and 3b).

The top spectrum (a) shows the γ rays in coincidence with three transitions: two of them (157 and 183 keV) are intense transitions between relatively low-lying levels of the band of simplex $-i$. The third imposed transition can be either one of two selected transitions located higher in this band (191 or 213 keV). This combination allows all the new γ rays attributed to the high-spin part of the band of simplex $-i$ to be observed. The last two γ-rays, at 463 and 472 keV, are clearly seen. One can notice the expected effects of the selected gates: extinction of the γ rays at 316 and 341 keV (bypassed by the 183.1 keV gate), and a strong presence of the γ rays at 132 and 187 keV. Apart from strong peaks corresponding to the x rays from lead and thorium, we can also see in the spectrum several γ rays attributed to transitions in the other main band (of simplex $+i$). This is due to two effects that are present during all the analysis: (i) as previously mentioned, the two main bands communicate, although the corresponding transitions are strongly converted and do not appear in the γ spectra; (ii) the two main bands are nearly degenerate (a typical feature of octupole bands), and in several cases a given γ-ray energy corresponds to different transitions. This is the case for instance for the transition at 157 keV that is even three times degenerate in the level scheme of ^{223}Th (this energy appears twice in the investigated band, hence the strong corresponding peak in the spectrum).

For the middle spectrum (b), the triple gate corresponds to transitions in the medium-spin part of the band of simplex $+i$. The specific combination of gates was again chosen in order observe most clearly γ rays attributed to the high-spin part of the two sequences 2a and 2b. Note the γ rays at 456 and 476 keV, issuing from the two highest levels, associated with the backbending phenomenon that will be discussed later. As previously, transitions belonging to the neighboring band can also be seen. The presence of the γ ray at 372 keV from the non-yrast structure is allowed by the combination of gates.

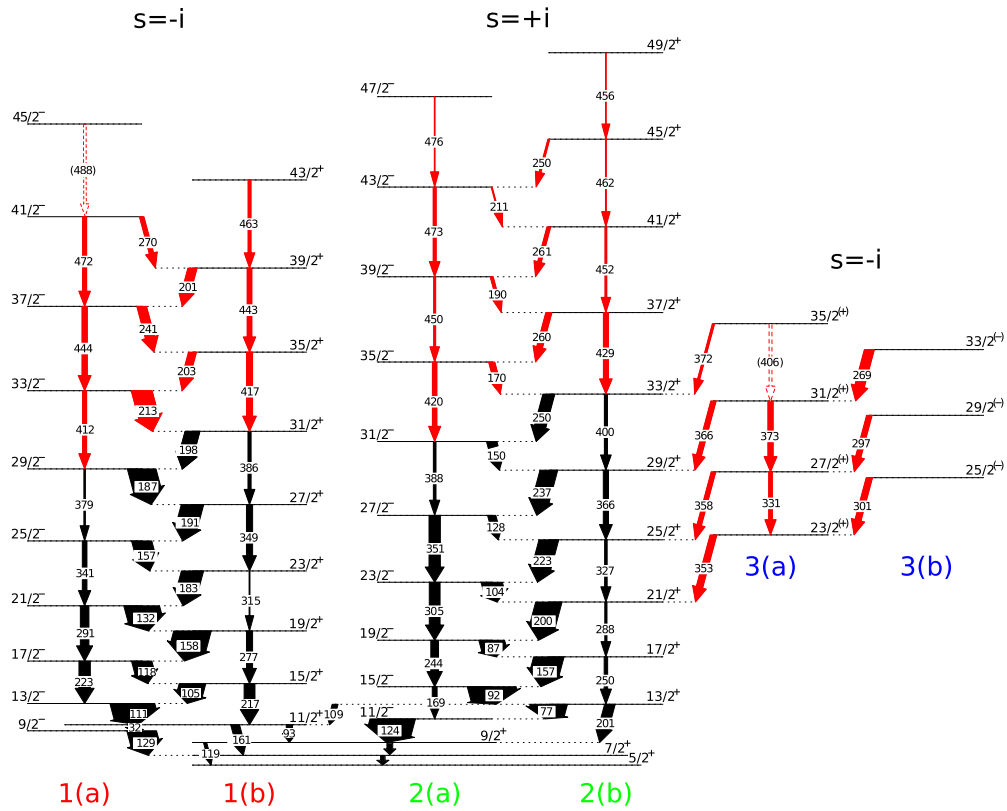

FIG. 2. Level scheme of ^{223}Th determined by γ-ray spectroscopy via the ^{208}Pb(^{18}O,$3n$)^{223}Th reaction. The widths of the arrows represents the γ-ray intensity of the transitions. The newly observed transitions are colored in red. The two main bands of alternating parity are classified in four sequences labeled 1a, 1b for the band of simplex $-i$ and 2a, 2b for the band of simplex $+i$ (each sequence has a fixed parity). A similar notation is used for the non-yrast structure, formed of two sequences labeled 3a and 3b. Spin-parity assignment for the main structure is based on the assumption of a $5/2^+$ ground state. Each of the two main bands presents intense stretched $E1$ intersequence transitions as well as stretched $E2$ intrasequence transitions. Strongly converted $M1$ transitions link these two bands: they are not represented here since they do not appear in γ spectroscopy. The parities of the non-yrast structure levels are tentative (see text).

The newly observed non-yrast structure is partially shown by the last spectrum (c). This structure communicates with the sequence 2b of the main band of simplex $+i$. The triple gate involves the 200 keV γ ray corresponding to the intense transition that link the non-yrast structure to the yrast sequences 2a and 2b. The other two conditions consist of conbinations of transitions inside the non-yrast structure, or between this structure and the main band. As a result, four γ rays associated with the non-yrast structure appear clearly in the spectrum (plus the γ ray at 331 keV that is less visible). Others appear when different sets of gates are imposed, but are suppressed here; for instance, the γ rays at 301, 366, and 372 keV are forbidden by the gate imposing the coincidence with γ rays at 331 or 373 keV. The coincidence required with 353 or 358 keV γ rays blocks the presence of these two transitions in the spectrum since they are anticorrelated.

The intra-sequence transitions have been observed for sequence 3a but not for sequence 3b. Such transitions would correspond to γ-ray energies of 327 and 345 keV, but they are too weak to be evidenced by dedicated sets of gates. One can notice that a γ ray at 327 keV is present in spectrum (c), but this transition is forbidden by the gate requirement (331 or 373 keV), instead, it is due to a known transition in sequence 2b, that can occur if the cascade joins the main band at level $25/2^+$. This γ ray disappears in a double-gated spectrum showing γ rays in coincidence with 200 and 353 keV (cascades where the main band is joined at level $21/2^+$).

The parities of the non-yrast band are assigned tentatively, under the following assumptions: (i) the transitions linking the non-yrast structure (sequence 3a) to the main structure (sequence 2b) are of $M1$ type with $\Delta I = 1$, as is the case between the two main bands of opposite simplex (converted transitions linking 1a to 2a on one side and 1b to 2b on the other side, see [8]); (ii) the two sequences of the non-yrast structure communicate by stretched $E1$ transitions and have stretched $E2$ intrasequence transitions. This picture is supported by our R_{ADO} measurements, and is consistent with the observed γ intensities. $M1$ γ transitions from the non-yrast structure to the main sequence can be observed due to the large energy difference between linked levels, and are competing with $E2$ intrasequence transitions involving similar energy differences. The $E1$ transitions from 3b to 3a are strongly dominant over $E2$ intrasequence transitions in 3b that involve similar energy differences; this explains why the latter are not observed. This pattern is due to the upshift of the assumed negative-parity sequence 3b with respect to the positive-parity sequence 3a, which also leads to the absence of observed $E1$ transitions from

3a to 3b (due to the tiny energy difference between successive $\Delta I = 1$ levels).

B. Low-spin structures

As already mentioned, one consequence of octupole correlations is the appearance of low-lying positive- and negative-parity states forming sequences of opposite parity interconnected by strong $E1$ transitions. These sequences are arranged in rotational bands of alternating parity states, each band being associated to a simplex quantum number s [23,24]. The possible s values depend on the projection of the angular momentum on the symmetry axis, given by the quantum number K. In the case of an even-mass nucleus ($K = 0$), the favored value is $s = +1$ and only one alternating parity band shows up. For odd-mass nuclei with $K \neq 0$, the simplex can take two values $s = \pm i$, giving rise to the doubling of almost all states with respect to their parity [25,26]. This is what is observed in nuclei such as ^{219,223,225}Th [8,27,28] and also ^{221}Ra [29], where $K \geqslant 3/2$: two quasidegenerate bands appear. Let us notice that the case of odd-mass nuclei with $K = 1/2$ such as ^{221}Th is particular: one of the bands is shifted up due to Coriolis effects and no parity doubling appears, the level scheme being similar to that of even-even isotopes [[8,13], and references therein].

The unambiguous spin assignment of ground states in ^{221}Th, ^{223}Th, and ^{225}Th could still be debated depending on the coupling scenario used for the valence nucleon. For ^{221}Th, the $7/2^+$ level is accepted to be the ground state. Calculations predict a strong $K = 1/2$ component for the state, which leads to the lack of a parity doublet in the level scheme [13,30]. It is also the case for ^{227}Th which has a $K = 1/2$ ground state configuration. Concerning the ^{223}Th and ^{225}Th yrast configurations, it has been established that they are based on $K > 1/2$ configurations. High-lying octupole bands, which exhibit the features of an almost degenerate parity doublet, have been found in ^{221}Th and interpreted as based on the same $K = 5/2$ configuration as the yrast band in ^{223}Th [13].

The new band found in this work, composed of the sequences 3a and 3b in the level scheme of Fig. 2, could be compared to structures with good simplex quantum number and no parity doublet. One may then expect the band-head configuration to have a dominant $K = 1/2$ component. Such a scenario is also confirmed by calculations using the reflection-asymmetric mean-field theory with an average Woods-Saxon potential and a monopole pairing residual interaction [30]. The low-lying one-quasiparticle excitations are given for ^{221,223,225}Th isotopes together with two quantum numbers K and n_K, which order single-particle levels of the same K energetically from the bottom of the potential well. It appears that the first excited state in ^{221}Th is the one expected for the ^{223}Th yrast configuration, although the $K = 3/2$ ($n_k = 17$) orbital lies close in energy. The situation is different for ^{223}Th, for which the lowest excited state is clearly identified to have a $K = 1/2$ component, in agreement with what we have observed in our data set. For a given simplex, one way to study the nature of the configuration is to draw the ratio of rotational frequencies of the negative and positive parity bands $\omega(-)/\omega(+)$ as a function of angular momentum. The ratio is calculated using the following formula [20]:

$$\frac{\omega^-(I)}{\omega^+(I)} = 2\frac{E(I+1)^- - E(I-1)^-}{E(I+2)^+ - E(I-2)^+} \tag{3}$$

Figure 3 displays the ratio for all the bands observed in our data set. The two limits, corresponding to reflection-asymmetric rotor and rotation-aligned octupole vibration, are also represented. The low number of γ rays composing the new excited band suggests a stable octupole deformation for the band head, which may not be strong enough to survive at higher spins.

On the other hand, the previously known bands (1a, 1b, 2a, and 2b) show a more characteristic behavior that can be interpreted as the stabilization of a well pronounced octupole shape [1]. However, one can see that some curves do not converge strictly to the asymptotic static limit. With the new transitions established in this work, one can discuss the assumption in more detail.

C. Medium-spin structures

Another way to characterize the evolution of octupole correlations with spin is through the parity splitting—the energy difference between the negative parity states and the (interpolated) positive parity states for a given spin—defined by the following equation:

$$\delta E(I) = E(I)^- - \frac{(I+1)E(I-1)^+ + IE(I+1)^+}{2I+1} \tag{4}$$

The parity splitting is shown for several thorium isotopes in Fig. 4. It should be zero in the case of a rigid octupole rotor. It is frequently stated that static octupole shapes are stabilized by rotation, since the parity splitting approaches zero with increasing spin; however, for some bands the evolution does not stop at zero but instead oscillates around this limit (see ^{220,222}Th in Fig. 4). Frauendorf [31] has proposed to interpret such properties of the rotational bands as based on the condensation of rotational-aligned octupole phonons. As we follow up the yrast states, the number n of phonons in the condensate increases with the angular momentum I. Since the parity of the state is determined by n, the energies of the negative and positive parity states are alternatively affected by phonon alignment, as the energy levels associated with different values of n cross each other. The successive values of n involve changes in the sign of the parity splitting. Additional anharmonicities [32] cause interactions between levels of same n parity: two such levels do not cross but repel each other, with mixing occurring at the quasicrossing. This effect determines the way $\delta E(I)$ varies between two consecutive crossings by zero. The anharmonicity and interaction of the phonons increase with N. It softens the transitions associated with each change of the phonon number and attenuates the oscillations, which is evident by looking at the evolution from ^{220}Th to ^{224}Th in Fig. 4. Reviol *et al.* [13] have extended the study to odd-N nuclei. They concluded that the rotation-induced condensation of octupole phonons carries over to the odd-N nuclei even if the presence of an additional neutron in the core seems to reduce the fluctuations in the octupole degree of freedom. With our new data, we have been able to extend the

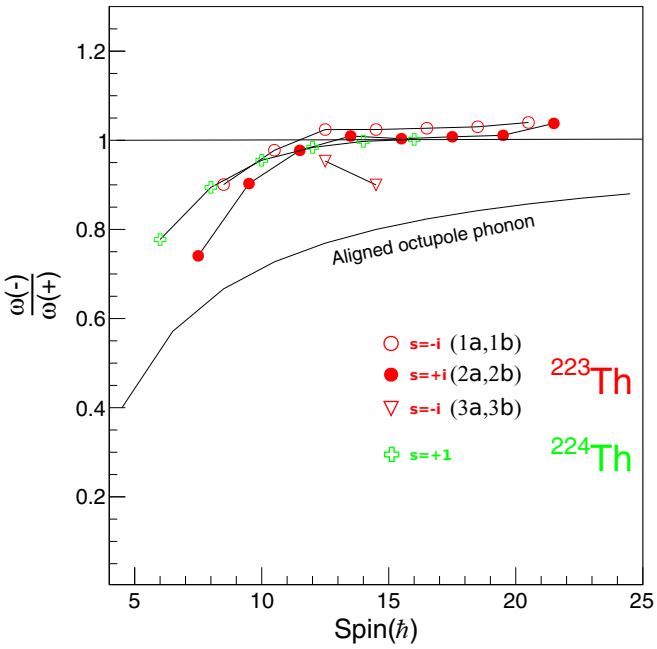

FIG. 3. Ratio between the rotational frequency of the negative and positive parity bands $\omega(\pi=-)/\omega(\pi=+)$ versus the angular momentum. A value of this ratio close to unity stands for a rigid reflection-asymmetric rotor. The behavior of a perfect aligned octupole phonon is also indicated.

parity splitting for ^{223}Th yrast sequences to higher spins (see Fig. 4). Concerning the $s=-i$ band, one can compare to what is observed for ^{222}Th, i.e., a crossing that brings back δE to positive values, in our case for spin $>15\hbar$. The amplitude of the last point is higher than the minimum and almost equal to the initial value. As well, for the $s=+i$ band, the tendency that can be guessed from previous data is confirmed. For spin $>12\hbar$, the curve grows slowly to reach about 0 for the latest value. It is worth noting that, except for the initial value, the differences in amplitude between the odd-mass ^{223}Th curves and the ^{222}Th core one are small. Unlike the parity splitting in ^{220}Ra [31], the data for ^{222,223}Th do not suggest any attenuation beyond the crossing of the two- to one-phonon band, i.e., once δE becomes positive again. It might be due to a weak, or delayed, mixing between the one- and three-phonon bands. Another possibility to explain such behavior arises more clearly from our data by looking at the highest spins in ^{223}Th (see below).

D. Backbending in the high-spin structure

As reported by Li *et al.* [4,5], the calculations indicate that ^{224}Th exhibits, at low spin, the critical point of a double phase transition, from spherical to quadrupole and from nonoctupole to octupole shape. At higher spin, one may then expect crossing of bands based on different shapes. An important difference between reflection-asymmetric and symmetric shapes concerns the effect of intruder states [33]: in thorium isotopes, high-j intruders are brought at the Fermi level, $j_{15/2}$ and $i_{13/2}$ for neutrons and protons, respectively. Without the octupole degree of freedom, such intruder states carry large alignment. As these orbitals slope down rapidly in energy with increasing rotational frequency, pair breaking is expected at relatively low spin along the yrast line. For $\beta_3 \neq 0$, since the octupole interaction mixes the intruder states with states of the major shell, such a large alignment is quenched. Indeed, without the octupole degree of freedom, one would expect sharp backbending at low spin in ^{224,226}Th yrast bands, which is not the case [34]. Using the cranked Woods-Saxon-Bogolyubov-Strutinsky method, Nazarewicz, Leander, and Dudek [35] performed the first theoretical exploration of the evolution of the octupole deformation with spin, in particular for ^{222}Th. As for ^{224,226}Th, configurations with spin alignment of $\nu j_{15/2}$ and $\pi i_{13/2}$ become, in the reflection-symmetric well, lowest already at low spin ($I \sim 12\hbar$); it is of course not confirmed by experimental data. However, including the octupole degree of freedom, they are able to reproduce the yrast line up to the highest spin observed. The calculations also predict a backbending around $26\hbar$, for a rotational frequency close to 0.23 MeV, due to the crossing with the four-quasiparticle $\nu(j_{15/2})^2\pi(i_{13/2})^2$ reflection-symmetric band.

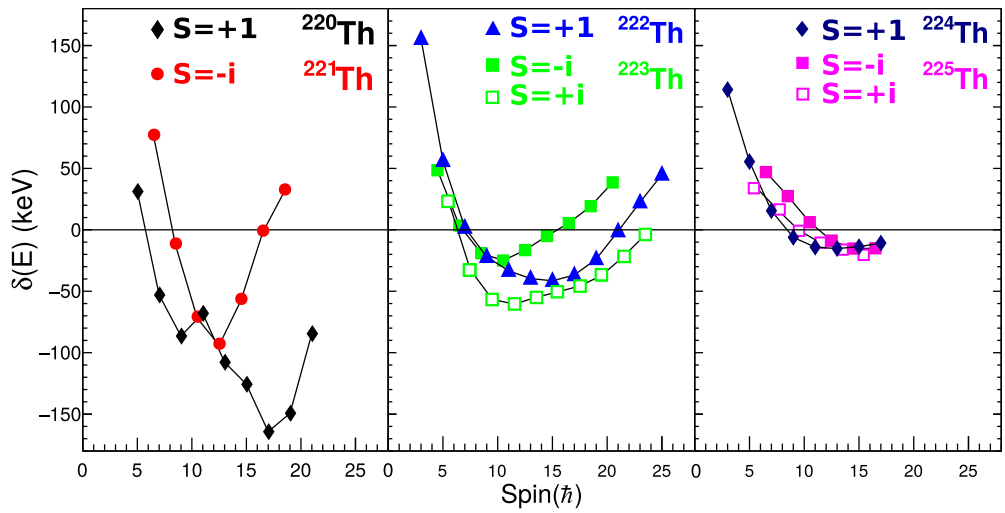

FIG. 4. Splitting between states with opposite parity within the same rotational band for various thorium isotopes as a function of spin.

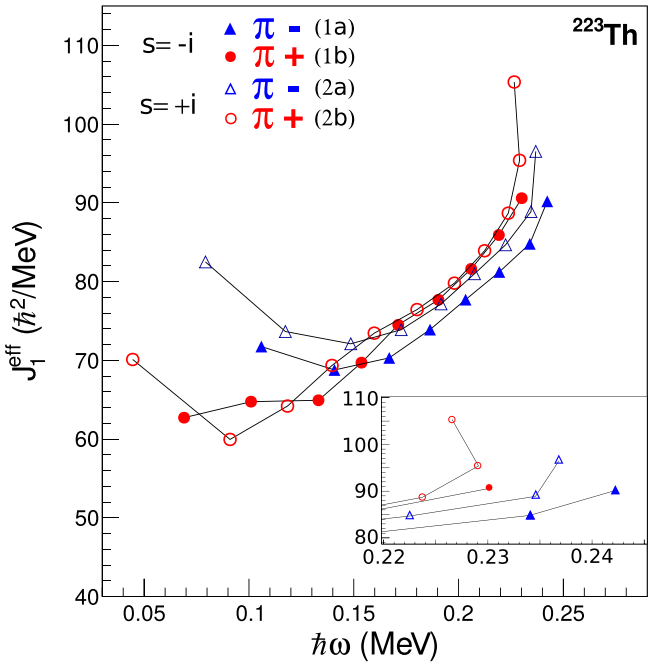

FIG. 5. Kinematic moment of inertia for both positive and negative parity states in ^{223}Th. The full (empty) symbols represent the sequence with simplex number $s = -i$ ($s = +i$). A backbending and an upbending arise from the positive and negative parity bands respectively, in the same simplex structure ($s = +i$) around rotational frequency of $\hbar\omega \simeq 0.23$ MeV.

Hints of such a shape transition, involving this four-quasiparticle configuration, have been reported. It is proposed as one possible explanation of the abrupt loss of intensity at spin $25\hbar$ in the ^{222}Th octupole band [36]. A similar feeding pattern in ^{221}Th leads to the same conclusion [13]. An upbend, which occurs at frequency between 0.18 and 0.19 MeV, has been observed in ^{225}Th for the $s = +i$ yrast band without being firmly assigned [28]. Coming back to our data set, the kinematic moments of inertia for the ^{223}Th yrast band are displayed in Fig. 5. The effective moment of inertia $J^{\text{eff}}_{(1)}$ as well as the rotational frequency ω were calculated using the standard technique described in Refs. [8,37]. It is well known that the negative parity sequences, at low spin, have a larger effective moment of inertia than the positive parity ones. It is related to a larger quadrupole deformation [38]. All the yrast sequences merge at medium frequencies around 0.15 MeV. Looking at the highest frequencies, one can see, for $s = +i$, a backbending for the positive parity band at 0.23 MeV and an upbend at a slightly greater frequency 0.24 MeV for the negative parity band. The $s = -i$ bands does not present such sudden changes. The rotational frequency at which the backbending is observed, 0.23 MeV, is very close to the value at which the shape transition in the ^{222}Th core is predicted [35]. To characterize more precisely the termination of the $s = +i$ band, it would be interesting to clearly identify the interacting band, as has been done for another octupole band in ^{150}Sm [39]. It seems, however, beyond the limits of what we are able to observe in our data sets.

IV. CONCLUSIONS

Shape transitions in the actinide region, involving the octupole degree of freedom, have been the object of several theoretical studies leading to the prediction of band-crossings occurring at high spin. In this paper we report on the first experimental evidence of such a crossing in the odd nucleus ^{223}Th, based on the new determination of its level scheme up to very high spin. An experiment, performed with EUROBALL IV, has indeed allowed us to extend our knowledge on the structure of this nucleus, since the pioneer work by Dahlinger *et al.* in the 1980s. The recent progress realized in γ-spectroscopy experiments comes from the use of multidetector arrays involving a large number of germanium crystals, together with fast electronics for data acquisition; the detection efficiency at high multiplicity has been substantially increased, yielding high-statistics data sets. Several features have emerged from our study of the newly identified ^{223}Th levels. A new structure has been identified and tentatively assigned to an octupole rotational band based on a $K = 1/2$ configuration. Concerning the yrast structure composed of four sequences, (i) the study of parity splitting has been extended and shows oscillations as expected in case of condensation of rotational-aligned octupole phonons, and (ii) a backbending and upbending have been observed in the $s = +i$ sequences, respectively, at spin-parity $49/2^+$ and $47/2^-$. The predicted shape transition from reflection-asymmetric to reflection-symmetric shape in the ^{222}Th core is emphasized to be a candidate for such a sudden band termination. This transition could also explain the absence of attenuation at high spin of the parity-splitting oscillations for ^{222,223}Th nuclei. To characterize more precisely the expected four-quasiparticle reflection-symmetric configuration that becomes yrast after the transition, it would be of considerable interest to perform measurements at even higher spin in the ^{222,224}Th isotopes and in the odd ^{223}Th nucleus. as was done in the $Z \simeq 88$, $N \simeq 56$ region of octupole deformation. However, for the actinide region, this represents a significant experimental challenge in terms of detection efficiency of transitions from weakly populated levels at very high spin. The role of the competition with fission should also be considered in discussing the possibility to observe such transitions. On the other hand, our study also opens the way to further investigations of shape transitions at high spins in the neighboring actinides, where evidence of such crossings, if they happen at smaller rotational frequencies, could be accessible with the current arrays and would bring valuable information. It will be also instructive to compare experimental results with new theoretical investigations of rotational bands including the octupole degree of freedom.

ACKNOWLEDGMENTS

The authors thank all the persons having participated in the EB-02/17 EUROBALL IV experiment devoted to the fission fragments, in which the data on ^{223}Th were recorded. The EUROBALL project was a collaboration between France, United Kingdom, Germany, Italy, Denmark and Sweden. This

work was supported in part by EU Contract No. HPRI-CT-1999-00078. We thank also all the persons having participated in the JUROGAM II experiment labeled as J16 whose first aim was to study the "$\alpha + {}^{208}$Pb" structure. If it were not for the first results on ^{223}Th found in this experiment, we would have not worked on the EUROBALL IV dataset. The authors also thank the GAMMAPOOL European Spectroscopy Resource for the loan of the detectors for the JUROGAM II array. This work was partially supported by the EU-FP7 Integrating Activities Project ENSAR (No. 262010), by the Academy of Finland and University of Jyväskylä within the Centre of Excellence program.

[1] P. A. Butler and W. Nazarewicz, Rev. Mod. Phys. **68**, 349 (1996).
[2] L. Gaffney and P. Butler, Nature (London) **497**, 199 (2013).
[3] P. A. Butler, J. Phys. G: Nucl. Part. Phys. **43**, 073002 (2016).
[4] Z. P. Li, J. Phys. G: Nuclear Part. Phys. **43**, 024005 (2016).
[5] Z. P. Li, B. Y. Song, J. M. Yao, D. Vretenar, and J. Meng, Phys. Lett. B **726**, 866 (2013).
[6] S. E. Agbemava, A. V. Afanasjev, and P. Ring, Phys. Rev. C **93**, 044304 (2016).
[7] I. Ahmad and P. A. Butler, Annu. Rev. Nucl. Part. Sci. **43**, 71 (1993).
[8] M. Dahlinger, E. Kankeleit, D. Habs, D. Schwalm, B. Schwartz, R. S. Simon, J. D. Burrows, and P. A. Butler, Nucl. Phys. A **484**, 337 (1988).
[9] A. Astier, P. Petkov, M.-G. Porquet, D. S. Delion, and P. Schuck, Phys. Rev. Lett. **104**, 042701 (2010).
[10] A. Astier and M.-G. Porquet, Un noyau de polonium d'evoile sa structure alpha, Images de la physique, CNRS, 2011, http://www.cnrs.fr/publications/imagesdelaphysique/couv-PDF/IdP2010/12_noyau_polonium_alpha.pdf.
[11] A. Astier, P. Petkov, M.-G. Porquet, D. Delion, and P. Shuck, Eur. Phys. J. A **46**, 165 (2010).
[12] S. K. Tandel, M. Hemalatha, A. Y. Deo, S. B. Patel, R. Palit, T. Trivedi, J. Sethi, S. Saha, D. C. Biswas, and S. Mukhopadhyay, Phys. Rev. C **87**, 034319 (2013).
[13] W. Reviol, R. V. F. Janssens, S. Frauendorf, D. G. Sarantites, M. P. Carpenter, X. Chen, C. J. Chiara, D. J. Hartley, K. Hauschild, T. Lauritsen, A. Lopez-Martens, M. Montero, O. L. Pechenaya, D. Seweryniak, J. B. Snyder, and S. Zhu, Phys. Rev. C **90**, 044318 (2014).
[14] J. Simpson, Z. Phys. A **358**, 139 (1997).
[15] J. Eberth, Nucl. Instrum. Methods A **369**, 135 (1996).
[16] G. Duchene, Nucl. Instrum. Methods A **432**, 90 (1999).
[17] D. C. Radford, Nucl. Instrum. Methods A **361**, 297 (1995).
[18] N. Amzal *et al.*, Acta. Phys. Pol. B **30**, 681 (1999).
[19] S. Ahmad, W. Klempt, R. Neugart, E. Otten, K. Wendt, C. Ekstriim, and T. I. Collaboration, Phys. Lett. B **133**, 47 (1983).
[20] W. Nazarewicz and P. Olanders, Nucl. Phys. A **441**, 420 (1985).
[21] T. H. Hoare, P. A. Butler, G. D. Jones, M. Loiselet, O. Naviliat-Cuncic, J. Vervier, M. Dahlinger, A. M. Y. El-Lawindy, R. Wadsworth, and D. L. Watson, J. Phys. G: Nucl. Part. Phys. **17**, 145 (1991).
[22] Z. Kalaninová, S. Antalic, F. P. Heßberger, D. Ackermann, B. Andel, B. Kindler, M. Laatiaoui, B. Lommel, and J. Maurer, Phys. Rev. C **92**, 014321 (2015).
[23] A. Bohr and B. Mottelson, *Nuclear Structure II* (Benjamin, Reading, MA, 1975).
[24] S. Frauendorf, Rev. Mod. Phys. **73**, 463 (2001).
[25] R. R. Chasman, Phys. Lett. B **96**, 7 (1980).
[26] S. Cwiok and W. Nazarewicz, Phys. Lett. B **224**, 5 (1989).
[27] W. Reviol, D. G. Sarantites, C. J. Chiara, M. Montero, R. V. F. Janssens, M. P. Carpenter, T. L. Khoo, T. Lauritsen, C. J. Lister, D. Seweryniak, S. Zhu, O. L. Pechenaya, and S. G. Frauendorf, Phys. Rev. C **80**, 011304 (2009).
[28] J. R. Hughes, R. Tölle, J. D. Boer, P. A. Butler, C. Günther, V. Grafen, N. Gollwitzer, V. E. Holliday, G. D. Jones, C. Lauterbach, M. Marten-Tölle, S. M. Mullins, R. J. Poynter, R. S. Simon, N. Singh, R. J. Tanner, R. Wadsworth, D. L. Watson, and C. A. White, Nucl. Phys. A **512**, 275 (1990).
[29] J. Fernández-Niello, C. Mittag, F. Riess, E. Ruchowska, and M. Stallknecht, Nucl. Phys. A **531**, 164 (1991).
[30] S. Cwiok and W. Nazarewicz, Nucl. Phys. A **529**, 95 (1991).
[31] S. Frauendorf, Phys. Rev. C **77**, 021304 (2008).
[32] P. von Brentano, N. V. Zamfir, R. F. Casten, W. G. Rellergert, and E. A. McCutchan, Phys. Rev. C **69**, 044314 (2004).
[33] W. Nazarewicz, P. Olanders, I. Ragnarsson, J. Dudek, and G. A. Leander, Phys. Rev. Lett. **52**, 1272 (1984).
[34] P. Schüler, Ch. Lauterbach, Y. Agarwal, J. D. Boer, K. Blume, P. Butler, K. Euler, C. Fleischmann, C. Gnther, E. Hauber, H. Maier, M. Marten-Tlle, C. Schandera, R. Simon, R. Tlle, and P. Zeyen, Phys. Lett. B **174**, 241 (1986).
[35] W. Nazarewicz, G. A. Leander, and J. Dudek, Nucl. Phys. A **467**, 437 (1987).
[36] J. F. Smith, J. F. C. Cocks, N. Schulz, M. Aïche, M. Bentaleb, P. A. Butler, F. Hannachi, G. D. Jones, P. M. Jones, R. Julin, S. Juutinen, R. Kulessa, E. Lubkiewicz, A. Płochocki, F. Riess, E. Ruchowska, A. Savelius, J. C. Sens, J. Simpson, and E. Wolf, Phys. Rev. Lett. **75**, 1050 (1995).
[37] R. Bengtsson and S. Frauendorf, Nucl. Phys. A **327**, 139 (1979).
[38] P. Bonche, P. H. Heenen, H. Flocard, and D. Vautherin, Phys. Lett. B **175**, 387 (1986).
[39] W. Urban, J. C. Bacelar, and J. Nyberg, Acta. Phys. Pol. B **32**, 2527 (2001).